Post-annealing effect on the structural and mechanical properties of multiphase zirconia films deposited by a plasma focus device

I. A. Khan[a)†], R. S. Rawat[b)], R. Ahmad[c)], and M. A. K. Shahid[a)]

[a)] *Department of Physics, Government College University, 38000 Faisalabad, Pakistan*
[b)] *National Institute of Education, Nanyang Technological University, Singapore 637616, Singapore*
[c)] *Department of Physics, GC University, 54000 Lahore, Pakistan*

(Received 27 March 2013; revised manuscript received 14 May 2013)

Nanostructured multiphase zirconia films (MZFs) are deposited on Zr substrate by the irradiation of energetic oxygen ions emanated from a plasma focus device. The oxygen operating gas pressure of 1 mbar (1 bar $= 10^5$ Pa) provides the most appropriate ion energy flux to deposit crystalline ZrO_2 films. X-ray diffraction (XRD) patterns reveal the formation of polycrystalline ZrO_2 films. The crystallite size (CS), crystal growth, and dislocation densities are attributed to increasing focus shots, sample axial distances, and working gas pressures. Phase and orientation transformations from t-ZrO_2 to m-ZrO_2 and c-ZrO_2 are associated with increasing focus shots and continuous annealing. For lower (200 °C) annealing temperature (AT), full width at half maximum (FWHM) of diffraction peak, CS, and dislocation density (δ) for (020) plane are found to be 0.494, 16.6 nm, and 3.63×10^{-3} nm^{-2} while for higher (400 °C) AT, these parameters for (111) plane are found to be 0.388, 20.87 nm, and 2.29×10^{-3} nm^{-2}, respectively. Scanning electron microscope (SEM) results demonstrate the formation of rounded grains with uniform distribution. The estimated values of atomic ratio (O/Zr) in ZrO_2 films deposited for different axial distances (6 cm, 9 cm, and 12 cm) are found to be 2.1, 2.2, and 2.3, respectively. Fourier transform infrared (FTIR) analysis reveals that the bands appearing at 441 cm^{-1} and 480 cm^{-1} belong to m-ZrO_2 and t-ZrO_2 phases, respectively. Maximum microhardness (8.65 ± 0.45 GPa) of ZrO_2 film is ~ 6.7 times higher than the microhardness of virgin Zr.

Keywords: zrconia, phase transformation, XRD, SEM, Fourier transform infrared analysis

PACS: 73.50.Lw, 68.60.Bs, 68.55.J−, 61.72.−y **DOI:** 10.1088/1674-1056/22/12/127306

1. Introduction

Zirconium oxide (ZrO_2), commonly known as zirconia, films have attracted huge attention as an important ceramic material because of their enhanced optical, chemical, and mechanical properties. High chemical stability, hardness, dielectric constant and index of refraction and low absorption of light make it an attractive material. ZrO_2 films have been utilized for a wide range of applications like wear resistant coatings, protective coating for optical mirrors and filters, thermal-barrier coatings, and high temperature fuel cells and oxygen detectors.[1–5] Moreover, ZrO_2 films have been employed in many engineering applications like automobile engine parts.[1–5] Additionally, materials (HfO_2 and ZrO_2) of high dielectric ($k \sim 20$) constant have been considered as SiO_2 substitutes, fundamentally due to their superior physical and electrical properties. Some leading companies are also using ZrO_2 as a dielectric material for metal–oxide semiconductor applications. ZrO_2 film, which is thermodynamically stable with respect to solid state reaction with silicon, is a promising candidate for SiO_2 replacement. It has a large band gap (~ 5.8 eV) and high dielectric constant ($k \sim 20$).[6–10] Actually, ZrO_2 exhibits various structural polymorphs; the most familiar are monoclinic, tetragonal, and cubic phases. Due to high fracture resistance, tetragonal phase has been the preferred material for wear and mechanical application while cubic phase is a diamond stimulant because of its high refractive index. Addition of trivalent and tetravalent dopants in ZrO_2 films is known to stabilize these metastable phases by creating oxygen vacancies to energetically favor structure. Cubic phase of ZrO_2 is mostly produced by the addition of up to 20% trivalent stabilizer oxides such as yttria or ceria.[11]

To deposit such types of important materials, various deposition techniques like ion beam assisted deposition, liquid thermal spray synthesis, ion implantation, and sol–gel[12–15] are being employed. However, deposition of ZrO_2 films at low temperatures has become more important and valuable in thin film industry because it eliminates the requirement of high substrate temperature which reduces the manufacturing cost. Moreover, the deposition of different polymorphs like monoclinic, tetragonal, and cubic phases of ZrO_2 without the addition of trivalent and tetravalent dopants also reduces the manufacturing cost but it is necessary to use high purity source material and impurities free environment.

Plasma focus (PF) offers a simple, cost effective and promising deposition technique, in which the electrical energy stored in the capacitor bank is rapidly converted into plasma energy resulting in the formation of short lived but hot (~ 1 keV–2 keV) and dense ($\sim 10^{25}$ m^{-3}–10^{26} m^{-3}) plasma

*Project supported by the Higher Education Commission of Pakistan.
†Corresponding author. E-mail: ejaz_phd@yahoo.com
© 2013 Chinese Physical Society and IOP Publishing Ltd

column. It is a source of neutrons (in the case of deuterium gas operation), X-rays, highly energetic ions, and relativistic electrons.[16–18] These energetic ions and hot dense plasma have been used to deposit thin films of different materials like TiC, TiN, ZrN, ZrON, and ZrAlON.[19–29] In the present work, we employed the PF deposition technique to deposit multiphase zirconia films (MPFs) at room temperature. The MZFs deposited on Zr substrate are characterized by X-rays diffraction (XRD), field emission scanning electron microscope (FE-SEM), energy dispersive X-rays (EDX) spectroscopy, Fourier transformed infrared (FTIR) spectroscopy, and Vickers microhardness techniques in order to explore the film surface properties like crystal structure, crystallite size, surface morphology, grain size, elemental concentrations, and microhardness. The post annealing effect on multiphase zirconia film deposited using 10 focus shots at 1-mbar oxygen ambient pressure and at the axial deposition distance of 6 cm is also examined by the above-mentioned characterization techniques.

2. Experimental setup

Nanostructured MZFs are deposited on Zr substrate at room temperature using low energy Mather-type PF device, powered by a single Maxwell 30 μF, 15 kV; fast discharging capacitor with a maximum storage energy of 3.3 kJ. The details of PF facility are provided elsewhere.[24–31] The shot-to-shot interval of PF operation is 3 min. An extremely hot dense focused plasma column[16] is formed in front of central electrode during the radial collapse phase of PF operation. Pinch plasma temperature gets high enough to completely ionize the filling gas species. Sausage instabilities are developed resulting in an induced electric field which accelerates oxygen ions towards the top plate of the chamber while relativistic electrons towards the anode.[32] Engraved anode is used in order to minimize the impurities of anode material which can be ablated by relativistic electron beam bombardment. High voltage signals are recorded using fast response high voltage probes on Tektronix (TDS 3054B 500 MHz) oscilloscope. A stainless steel shutter is used to avoid the sample exposure during first few weak focus shots. The Zr substrate samples, used for ion irradiation, are prepared in the form of disk with a diameter of 10 mm and thickness of 4 mm. The substrate surface is polished with SiC abrasive paper of 2000 grid, ultrasonically cleaned in acetone for 30 min and finally washed with deionized water.

The basic mechanism behind the formation of MZFs can be illustrated as follows: the energetic oxygen ions emanated during the radial collapse phase of PF operation reach the substrate surface first, causing etching and hence cleaning the substrate surface prior to the deposition of MZFs. However, the ions are emitted in more than one bunches with a period of a few to tens of nanoseconds.[33] During ion irradiation, substrate surface's transient temperature increases, resulting in substrate sputtering, creating substrate plasma which reacts with ambient oxygen species to form MZFs. It is well known that total energy delivered to the substrate surface increases with the increase of focus shots since energy deliverance to the substrate surface is associated with the total number of incorporated ions and the total number of these ions increases with increase of focus shots. Therefore, increasing number of incorporated ions (due to the larger number of PF deposition shots) will change the film surface properties like phases, crystallinity, crystallite size, residual stresses, shape and size of grains, surface morphology, compactness, elemental composition, and chemical bonding. Moreover, the nucleation and growth of different phases of zirconia depend on the total ion energy flux delivered to the substrate surface, energy of the sputtered Zr, and ionized oxygen species. The sputtered Zr species react with the subsequent incoming oxygen ions (during the next bunches of the same focus shots) which enhances the nucleation as well as growth rate of MZFs. Additionally, in order to investigate the annealing effect on the film surface properties, we anneal the as-deposited MPFs at two different (200 °C and 400 °C) temperatures.

3. Structural analysis

XRD analysis is employed to investigate the structural information of MZFs. The average crystallite size (CS) is calculated by using Scherrer formula[34,35]

$$CS = \frac{k\lambda}{w\cos\theta},$$

where numerical constant $k = 0.94$, wavelength of incident radiation $\lambda = 1.54$ Å, and w is the full width at half maximum (FWHM) of the diffraction peak. The strain (ε) developed in a plane of zirconia is estimated from the equation[36,37]

$$\varepsilon = \frac{w\cos\theta}{4}.$$

The dislocation density (δ), defined as the length of dislocation lines per unit volume of the crystal, is estimated from the relation[36,37]

$$\delta = \frac{1}{(CS)^2}.$$

4. Results and discussion

4.1. Voltage signal analysis

Figure 1 demonstrates the intensities of high voltage probe signals recorded for different oxygen gas pressures of 1, 2, and 3 mbar. It is worth noticing that oxygen ions are emitted in more than one bunch since each high voltage signal consists of more than one peak. This result accords well with the result in Ref. [33]. Moreover, the ions belonging to different bunches are of different energies as typically the ions coming out from the first bunch are energetic comparatively. It is well known that ion energy flux is associated with the focusing efficiency of voltage signal; the higher the voltage probe

peak, the more energetic the ions will be. However, the estimation of ion beam parameters like ion velocity, ion energy, and ion number density are found in the literature.[26–28,38,39] For more detailed emission characteristics of ions emanated from plasma focus devices, the readers are advised to refer to the recent work by Lee and Saw.[40] It is found that the estimated ions energy ranges from few tens of keV to few MeV and the ion number density is found to be the order of 10^{19} m^{-3}. Additionally, the energy of the irradiated ions is associated with the working gas pressure since the intensity of high voltage probe signal depends on working gas pressure. Figure 1 reveals that voltage signal recorded for 2-mbar working gas pressure gives more ion energy flux because the peak in the voltage probe signal is comparatively intense. While XRD results (discussed later) exhibit that ion energy flux for 1-mbar pressure is more suitable for the growth of MZFs.

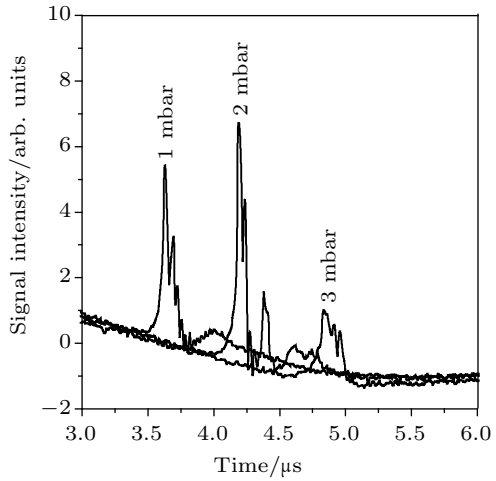


Fig. 1. High voltage probe signals recorded at different working gas pressures (1 mbar, 2 mbar, and 3 mbar).

4.2. XRD analysis

Figure 2 exhibits XRD patterns of MZFs deposited for different number of focus shots (5, 10, 15, and 20), while the sample axial distance (6 cm) and working gas pressure (1 mbar) are kept constant. XRD patterns show that virgin Zr has major diffraction peak appearing at 2θ value of 36.85°. For 5 focus shots, diffraction peaks related to Zr become weaker and broader. The weakening of Zr peak can be attributed to the partial amorphization of top Zr surface by energetic ion irradiation as well as to the partial oxide (zirconia) phase formation. The amorphization of bulk target surface has also been reported earlier in plasma focus irradiation.[41] The broadening of peaks can be attributed to nanostructurization of the exposed Zr surface. The absence of zirconia phase for 5 shot irradiation is due to insufficient oxygen ion and oxygen plasma treatment of the exposed Zr substrate. For 10 focus shots, the diffraction peaks appearing at 2θ values of 35° and 36.1° are related to t-ZrO_2 and m-ZrO_2 phases, respectively. It is clear that the growth of t-ZrO_2 phase is more than m-ZrO_2 since the peak intensity related to t-ZrO_2 phase is higher. For 15 focus shots, the peak intensity of t-ZrO_2 phase decreases while that of m-ZrO_2 phase increases. For 20 focus shots, again the growth of t-ZrO_2 phase is more than m-ZrO_2 since the peak intensity related to t-ZrO_2 phase is again higher. However, the broadening of diffraction peak indicates the formation of nanocrystallite of zirconia since crystallite size is inversely related to peak broadening. It is concluded that minimum ion dose (focus shots) for the better growth of t-ZrO_2 is about 10 focus shots.

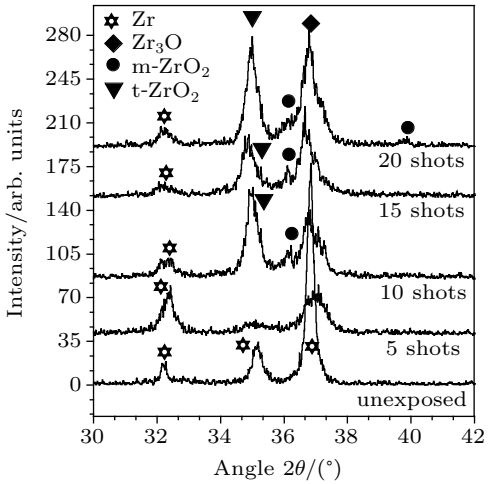


Fig. 2. XRD patterns of multiphase ZrO_2 films deposited for different focus deposition shots (5, 10, 15, and 20) at a fixed axial distance (6 cm) and working gas pressure (1 mbar).

Figure 3 shows XRD patterns of MZFs deposited for different axial distances (6, 9, and 12) while keeping the working gas pressure (1 mbar) and ion doses (10 focus shots) constant. For 6-cm axial distance, again the diffraction peak intensity of t-ZrO_2 phase is more than that of m-ZrO_2 phase. For 9-cm axial distance, intensities of the diffraction peaks related to t-ZrO_2 phase and m-ZrO_2 phase are smaller thereby indicates the formation of nanocrystallites. However, the development of three diffraction peaks related Zr_3O phase hinders the growth of t-ZrO_2 and m-ZrO_2 phases. For 12-cm axial distance, again t-ZrO_2 and m-ZrO_2 phases along with the formation of Zr_3O phase having different orientations are observed. However, the maximum growth of Zr_3O phase is observed due to its comparatively high peak intensity. Once more, it is concluded that maximum growth of zirconia (t-ZrO_2 and m-ZrO_2) is obtained for 6-cm axial distance. Moreover, most of the diffraction peaks are asymmetric which indicates the presence of defects and more broadened peaks indicating the formation of nanocrystallites. The variations in CS, ε, and δ with the increase of focus shots and sample axial distance are shown in Tables 1 and 2. This variation demonstrates that these parameters are directly related to the relative number of incorporated ions and their energies since ion energy decreases with increasing axial distance. Thus one can deposit MZFs of desired surface properties just by controlling the deposition parameters. The formations of nanocrystallites and the overlapping

of diffraction peaks confirm the development of micro-strains which are due to the lattice distortion and point defects developed in MZFs. Moreover, the mixing of phases improves the microhardness of the deposited MZFs.

Table 1. Structural parameters of t-ZrO_2 nanolayers for different numbers of focus shots.

Number of focus shots	FWHM	2θ	*CS*/nm	ε	$\delta/10^{-3}$ nm^2
10	0.475	34.97	17	0.113	3.46
15	0.532	34.88	16	0.127	3.91
20	0.464	34.99	18	0.111	3.09

Table 2. Structural parameters of t-ZrO_2 nanolayers for different sample axial positions.

Sample axials position	FWHM	2θ	*CS*/nm	ε	$\delta/10^{-3}$ nm^2
6	0.475	34.97	18	0.113	3.27
9	–	–	–		–
12	0.214	34.95	13.6	0.051	5.41

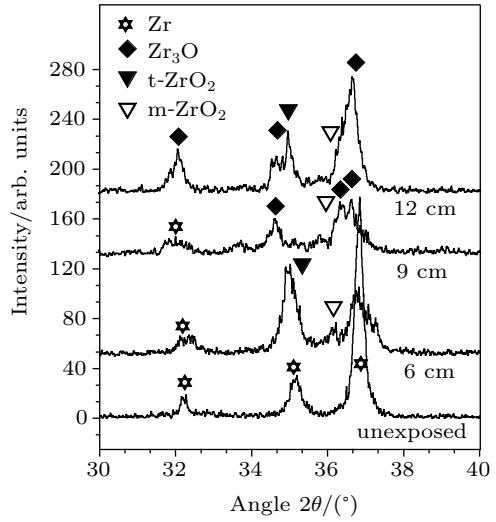


Fig. 3. XRD patterns of multiphase ZrO_2 films deposited for different (6, 9, and 12) axial positions at a fixed working gas pressure (1 mbar) and 10 focus deposition shots.

Figure 4 reveals the deposition of MZFs when the samples are exposed to different (1 mbar, 2 mbar, and 3 mbar) working gas pressures while the axial distance (6 cm) and ion doses (10 focus shots) remain constant. For 1-mbar pressure, the better growth of t-ZrO_2 and m-ZrO_2 phases is observed since their peak intensities are superior comparatively. For 2-mbar pressure, t-ZrO_2 phase is again observed but shows small crystallinity (weak peak intensity). For 3-mbar pressure, no diffraction peak related to t-ZrO_2 and m-ZrO_2 phases is observed. However, small changes in peak intensity of Zr phase are observed. Thus it is concluded that the nucleation and growth of t-ZrO_2 and m-ZrO_2 phases deposited for (i) 10 focus shots, (ii) 6-cm axial distance, and (iii) 1-mbar pressure are superior comparatively. Moreover, the variation in growth behavior of t-ZrO_2 and m-ZrO_2 phases is correlated with ion energy flux whereas the ion energy flux goes on decreasing by increasing the sample axial distance and working gas pressure. Results show that ion energy flux obtained for 1-mbar working gas pressure is more suitable for the nucleation and growth of MZFs. Now we come to discuss the annealing effect on the as-deposited zirconia film.

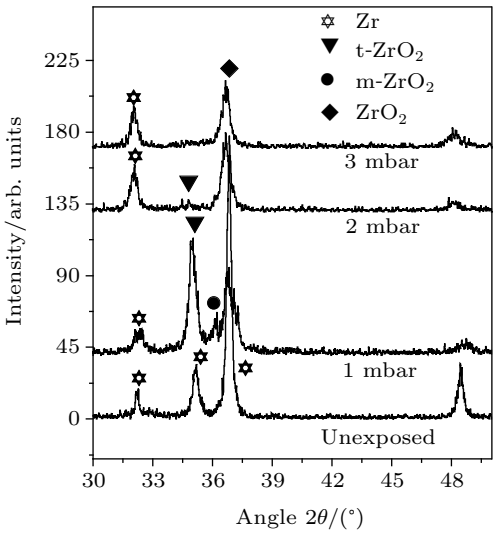


Fig. 4. XRD patterns of multiphase ZrO_2 films deposited at different working gas pressures (1 mbar, 2 mbar, and 3 mbar) for fixed axial distance (6 cm) and 10 focus deposition shots.

Figure 5 demonstrates the annealing (200 °C and 400 °C) effect on the as-deposited zirconia film. For annealing (200 °C) temperature, zirconia film grows along two different (020) and (102) orientations which are related to m-ZrO_2 phase. However, zirconia grows more along (020) orientation while (102) orientation of m-ZrO_2 phase is overlapped with Zr phase. This overlapping of diffraction peaks is due to the fact that the diffraction peaks are very close and have higher FWHM due to the formation of nanocrystallites. Moreover, it is obvious that t-ZrO_2 phase observed in the as-deposited zirconia film is converted into m-ZrO_2 phase during continuous annealing. Thus phase transformation from t-ZrO_2 to m-ZrO_2 is associated with continuous annealing. For annealing temperature (400 °C), all the diffraction peaks appearing in zirconia film annealed at lower temperature disappear with the development of new diffraction peaks (111), (−111), (102), and (210) which are related to m-ZrO_2 phase. However, m-ZrO_2 phase grows much along (111) orientation comparatively since its peak intensity is maximum. Additionally, a diffraction peak (111) related to c-ZrO_2 phase is also observed. It is interesting to note that the major content of zirconia film is still m-ZrO_2 phase but its orientation changes for higher AT. Thus orientation transformation of m-ZrO_2 phase occurs during continuous annealing. Moreover, reduction in Zr content (since diffraction peaks are weak and broaden) indicates that film thickness increases. Moreover, multiphase zirconia film which is free from t-ZrO_2 phase is observed for both ATs. It is concluded that t-ZrO_2 phase is not stable even at lower temperature while m-ZrO_2 is stable even at higher AT.

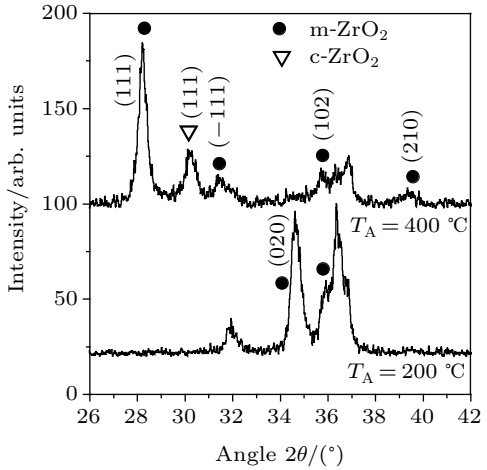


Fig. 5. XRD patterns of multiphase ZrO_2 films annealed at different temperatures (200 °C and 400 °C).

The overlapping of m-ZrO_2 and Zr phases, development of residual stresses, occurrence of new diffraction peaks, recrystallization of Zr phase, the formation of nanocrystallites, and phase and orientation transformations (from t-ZrO_2 to m-ZrO_2) are responsible for improving the microhardness value (discuss later). Additionally, the phase and orientation transformations are associated with AT. The estimated values of FWHM, *CS*, and δ for (020) plane observed at lower AT are found to be 0.494, 16 nm, and 3.63×10^{-3} nm^{-2} while these parameters for (111) plane observed at higher AT are found to be 0.388, 20.87 nm, and 2.29×10^{-3} nm^{-2}, respectively. These parameters along with the existence of more than one zirconia phase play an important role in improving the mechanical properties of MZFs.

Tian *et al.*[42] reported on the deposition of MZFs with electron beam evaporation when the substrate temperature was 573 K. They pointed out that zirconia film contains t-ZrO_2 phase before annealing. After annealing at 673 K, the peak intensity of t-ZrO_2 increases but when the zirconia film was annealed at 1064 K, peak intensity decreased along with the appearance of m-ZrO_2 phase. In our work, we deposit MZFs which contain both t-ZrO_2 phase and m-ZrO_2 phase by the irradiation of energetic oxygen ions at room temperature and no biasing was provided to the substrate. This reduces the deposition cost of MZFs. When the deposited zirconia film is annealed at 200 °C, t-ZrO_2 phase decomposes into m-ZrO_2 phase, confirming the phase transformation with improved crystallinity. The annealing at 400-°C temperature shows that m-ZrO_2 phase remains stable but grows along other orientation along with the formation of c-ZrO_2 phase. Tian[42] reported on the similar results but at higher AT.

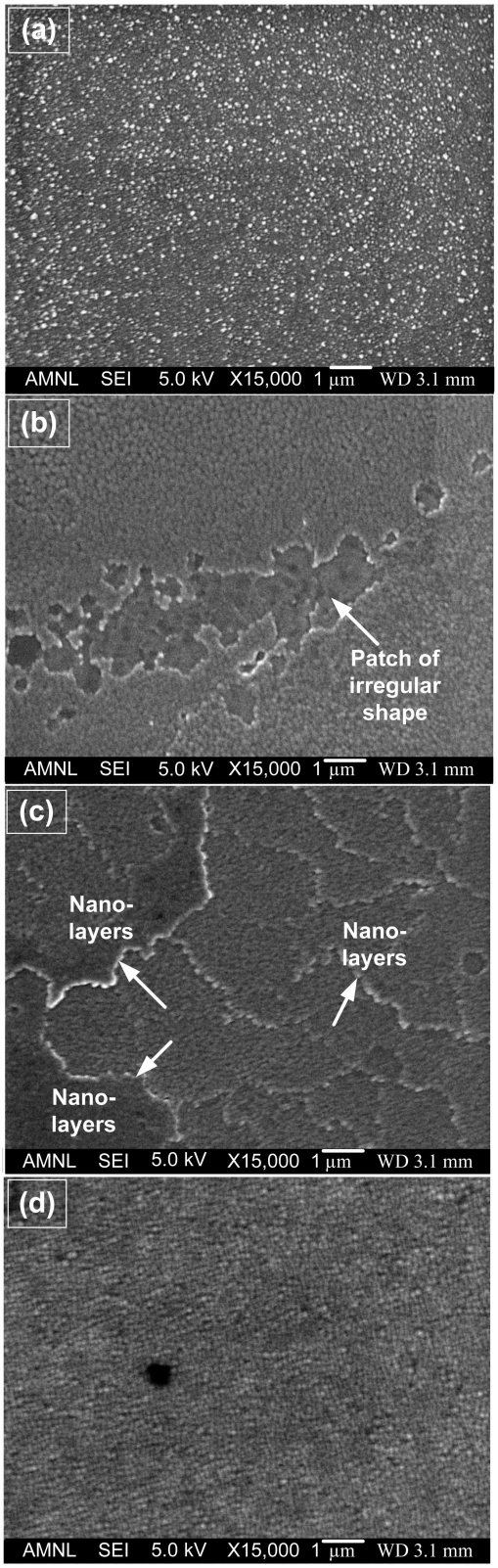


Fig. 6. Surface morphologies of multiphase ZrO_2 films deposited for different focus deposition shots: (a) 5, (b) 10, (c) 15, and (d) 20 focus shots at 1-mbar working gas pressure and an axial distance of 6 cm.

4.3. SEM analysis

Figure 6 exhibits the surface morphologies of MZFs deposited for different (5, 10, 15, and 20) focus shots by keeping the gas pressure (1 mbar) and source to substrate distance (6 cm) constant. For 5 focus shots, the deposited multiphase zirconia film demonstrates the formation of rounded

grains of 66 nm to 132-nm size (Fig. 6(a)). These rounded grains are distributed uniformly over the entire scanned area. Careful investigation reveals that rounded grains of smaller dimension distributed in the background of the upper zirconia film make the surface rough. Moreover, the zirconia film is not compact since grains are not close to each other. For 10 focus shots, the deposited zirconia film is compact and consists of many patches. These patches overlap with each other, confirming the formation of stacked layers of zirconia (Fig. 6(b)). However, due to highly compact nature of zirconia film it is difficult to estimate the size of the particles. For 15 focus shots, again compact zirconia film is observed, showing huge irregular patch (Fig. 6(c)) which again confirms the formation of multiphase zirconia film of two or more stacked layers. For 20 focus shots, an abrupt change in surface morphology of zirconia film is observed (Fig. 6(d)). Again rounded grains of $\sim$ 100-nm size are distributed uniformly in the entire scanned area.

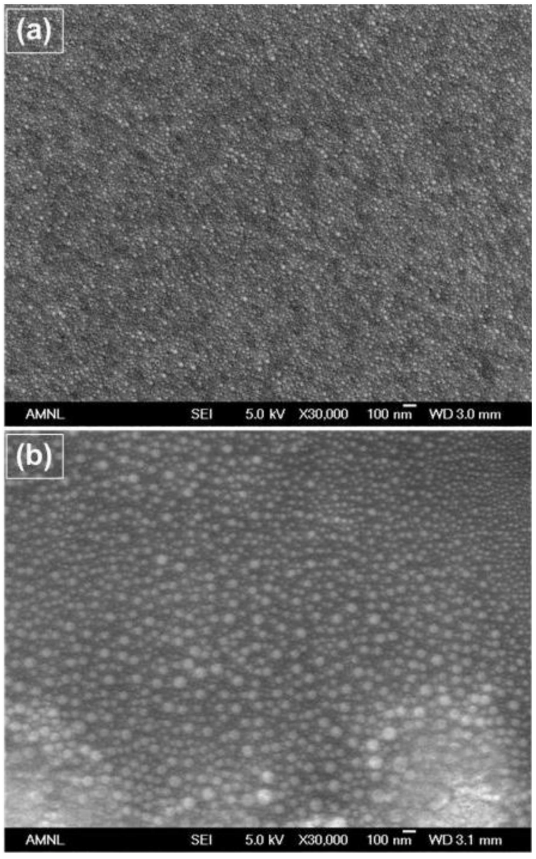


Fig. 7. SEM images of multiphase ZrO_2 films deposited at different axial positions: (a) 9 cm and (b) 12 cm, 1-mbar working gas pressure and with 10 focus deposition shots.

Figure 7 shows SEM images of MZFs deposited at different (9 cm and 12 cm) axial distances by keeping the working gas pressure (1 mbar) and focus shots (10) constant. Zirconia film deposited at 9-cm axial distance shows the formation of rounded grains ranging from 25 nm to 35 nm in size while for the deposition done at 12 cm the grain size ranges from 20 nm to 120 nm. It is well known that ion energy flux decreases with the increase of sample axial distance. Moreover, high energy ions have greater ability to diffuse into the substrate surface and transfer their energies which are absorbed by several particles, resulting in their better growth. Thus, the growth of different grains makes the surface rough. From the above results it is concluded that various surface properties like grain size, grain shape, grain distribution, film compactness, and formation of multi-layered zirconia films are attributed to ion energy flux which is controlled by the number of focus shots, sample axial distance, and working gas pressure.

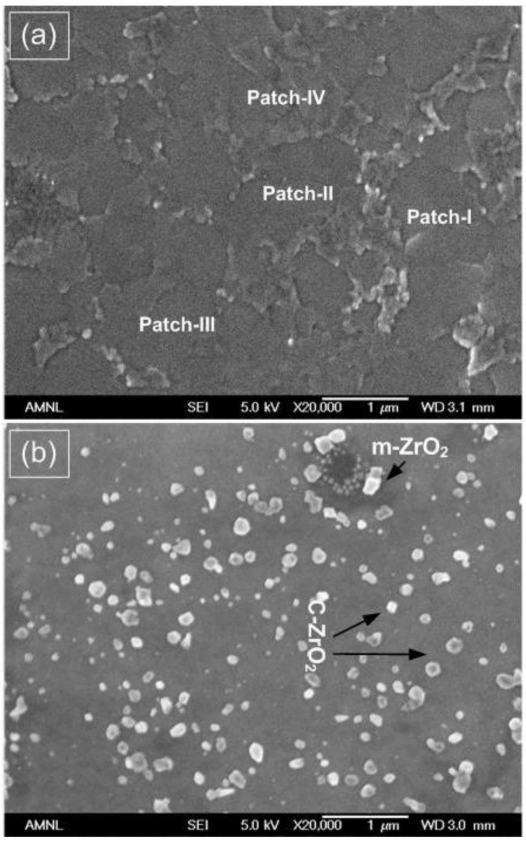


Fig. 8. Surface morphological features of multiphase ZrO_2 films annealed at different temperatures (a) 200 °C and (b) 400 °C.

Figure 8 demonstrates the morphological features of MZFs at annealing temperatures of 200 °C and 400 °C. The MZF (annealed at lower temperature) shows the formations of many patches, overlapping with each other. This confirms the deposition of multilayered multiphase zirconia film which is compact in nature. Multiphase zirconia film (annealed at higher temperature) shows the formation of particles of different shapes like cubic and monoclinic. The size of these particles ranges from 40 nm to 200 nm. During the phase transformation [from t-ZrO_2 to m-ZrO_2 phase (at lower AT)], multilayered multiphase zirconia films are formed, which is due to the rearrangement of two phases during continuous annealing. The re-crystallization of m-ZrO_2 (020) plane and development of m-ZrO_2 (111) plane indicate the orientation transformation. This indicates that m-ZrO_2 (020) plane does not remain stable at higher AT; however it grows along m-ZrO_2

(111) plane at higher AT. Thus the orientation transformation depends on continuous annealing. Moreover, microstructure of MZFs changes from a film that contains many patches into a film having particles of different shapes like cubic and monoclinic, which is due to the phase and orientation transformation during continuous annealing.

4.4. Quantitative elemental analysis

Figure 9 exhibits EDX spectrum of the as-deposited multiphase zirconia film, which confirms the presence of Zr (31.12 at.%) and oxygen (65.56 at.%). It is also found that Zr content decreases while oxygen content increases with the increase of sample axial distance. The values of ratio (O/Zr) in MZFs deposited for different (6 cm, 9 cm, and 12 cm) axial distances are found to be 2.1, 2.3, and 2.5, respectively. This increasing ratio (O/Zr) is associated with decreasing ion energy flux. The lower ion energy flux at higher distance of exposure is expected to result in lower average nanoparticle size, and due to less energy the agglomeration of neighboring nanoparticle is less probable. This will result in larger surface-to-volume ratio and hence the greater probability of oxidation.

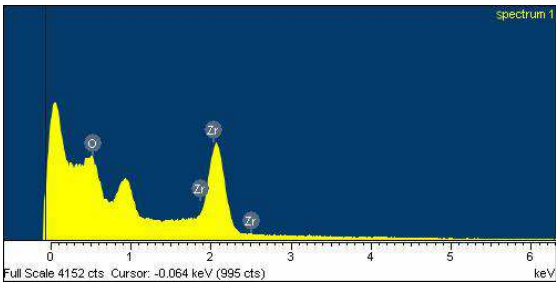


Fig. 9. (color online) EDX spectrum of multiphase ZrO_2 film deposited for 10 focus shots at axial distance of 6 cm and 1-mbar working gas pressure.

4.5. FTIR analysis

Figure 10 shows FTIR transmittance spectra of MZFs deposited for different (5, 10, 15, and 20) focus shots while keeping the sample axial distance (6 cm) and gas pressure (1 mbar) constant. For 5 focus shots, the transmittance band located at 441 cm^{-1} is related to Zr–O vibration mode of m-ZrO_2 phase.[37] It may be noted that XRD pattern of this sample does not show any diffraction peaks related to ZrO_2 phase. Thus XRD could not detect the small content of ZrO_2 while FTIR result confirms the presence of m-ZrO_2. For 10 focus shots, the transmittance band located at 480 cm^{-1} is related to Zr–O vibration mode of t-ZrO_2 phase.[37]

For 15 focus shots, the transmittance band located at 441 cm^{-1} is related to Zr–O vibration mode of m-ZrO_2 phase. Careful investigation reveals that t-ZrO_2 phase may also exist since the band related to m-ZrO_2 phase is more broaden which ranges from 430 cm^{-1} to 530 cm^{-1}. It means that t-ZrO_2 phase could not grow separately but co-exist with m-ZrO_2 phase. For 20 focus shots, the transmittance band is centered at 459 cm^{-1} and ranges from 430 cm^{-1} to 530 cm^{-1} which again confirms the co-existence of m-ZrO_2 and t-ZrO_2 phases. Moreover, shifting in the transmittance band position is also observed, which confirms the development of residual stress which is attributed to the formation of point defects and lattice distortions.

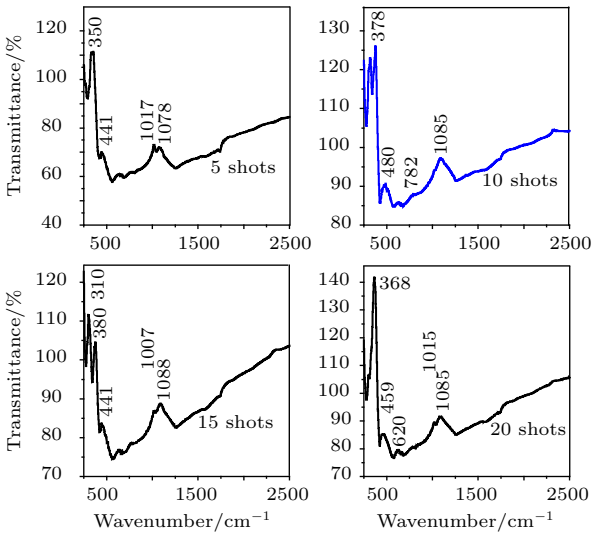


Fig. 10. (color online) FTIR transmittance spectra of multiphase ZrO_2 films deposited for different (5, 10, 15, and 20) focus deposition shots.

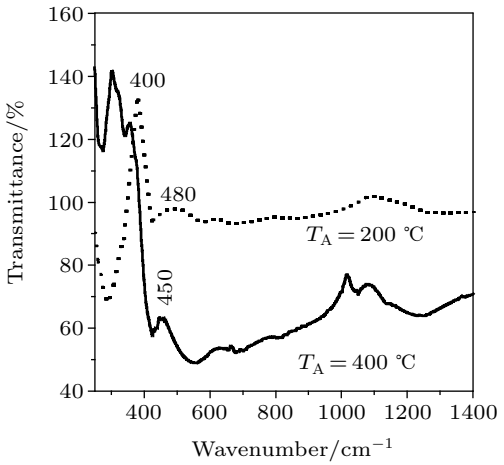


Fig. 11. FTIR transmittance spectra of multiphase ZrO_2 films annealed at different temperatures (200 °C and 400 °C).

Figure 11 shows FTIR transmittance spectra of multiphase zirconia annealed at different (200 °C and 400 °C) temperatures. For 200 °C annealing temperature, transmittance bands are observed at 400 cm^{-1} and 480 cm^{-1}. These bands are related to m-ZrO_2 and t-ZrO_2 phases, respectively; however, t-ZrO_2 phase is in small quantity due to weak band intensity. The band related to m-ZrO_2 phase is shifted towards lower values, indicating the presence of residual stresses which is due to the diffusion of oxygen species during continuous annealing. For 400 °C annealing temperature, the band related to m-ZrO_2 phase at 450 cm^{-1} is observed. This band

is, however, shifted towards higher values, indicating the presence of residual stress. Moreover, comparatively stress relaxation is observed for higher AT which is due to continuous annealing and orientation transformation of m-ZrO_2 phase.

4.6. Microhardness analysis

Figure 12 shows the values of surface microhardness (GPa) of MZFs deposited for different (5, 10, 15, and 20) focus shots keeping the sample axial (6 cm) distance and working gas pressure (1 mbar) constant. Five measurements (for 50 gf imposed load) are taken in order to estimate the average values of microhardness. The microhardness of MZFs increases with increasing number of focus shots. The maximum microhardness of MZFs deposited for 20 focus shots is found to be 8.65 ± 0.45 GPa which is ~ 6.65 times higher than the microhardness of virgin Zr. In one of our earlier work we showed that nitrogen content in zirconium nitride film increased with the increase in number of focus shots.[27] Thus we may say that oxygen content increases with the increasing number of focus shots and is one of the main reasons leading to the improvement of the microhardness of MZFs. Moreover, the increase in microhardness of MZFs could also be explained in terms of lattice distortion, defects, and vacancies which are associated with the total number of incorporated energetic ions. Actually, Zr lattice is distorted by the incorporation of oxygen ions interstitially and ions induced collision cascades create point defects. The lattice distortion, defects, and vacancies inhibit the mobility of dislocations, which improves the microhardness of multiphase zirconia films. Moreover, the development of different phases of zirconia and their nanocrystallites also increases the microhardness of MZFs. The co-existence of multiple zirconia phases is probably the other reason of enhancing the microhardness values of MZFs

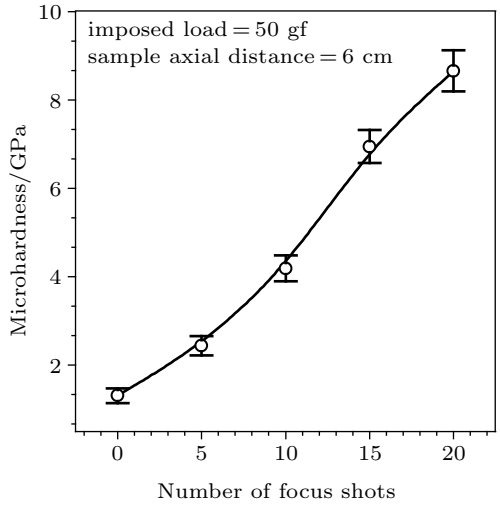


Fig. 12. Values of surface microhardness (GPa) of multiphase ZrO_2 films deposited for different (5, 10, 15, and 20) focus deposition shots for constant (i) sample axial (6 cm) distance and (ii) at 1-mbar working gas pressure.

Figure 13 exhibits the values of surface microhardness (GPa) of MZFs deposited at different sample axial (6 cm, 9 cm, and 12 cm) distances keeping the number of focus shots (10) and working gas pressure (1 mbar) constant. The values of microhardness of MPFs decrease from $\sim 4.2 \pm 0.23$ GPa to $\sim 3.6 \pm 0.08$ GPa with the increase of sample axial distances. A sharp decrease in microhardness is observed for 9-cm axial distance while slow decrease in microhardness is observed for 12-cm axial distance, which is due to the decrease in ion energy flux with the increase of sample axial distance. Thus the reductions in lattice distortion and point defects reduce the microhardness values of MZFs comparatively. Only low energy ions can reach the Zr substrate, the sputtered Zr species of comparatively low energy react with the available oxygen species to nucleate zirconia which is not crystalline but overlaps with ZrO_3 phase. The overlapping of diffraction peaks and the formation of nanocrystallite of ZrO_2 and ZrO_3 phases increase the microhardness of MZFs. Thus, decreasing the content of Zr, oxygen, m-ZrO_2 phase, and t-ZrO_2 phase is the major reason of reducing the microhardness values of MZFs comparatively but still it is more than that of the virgin Zr.

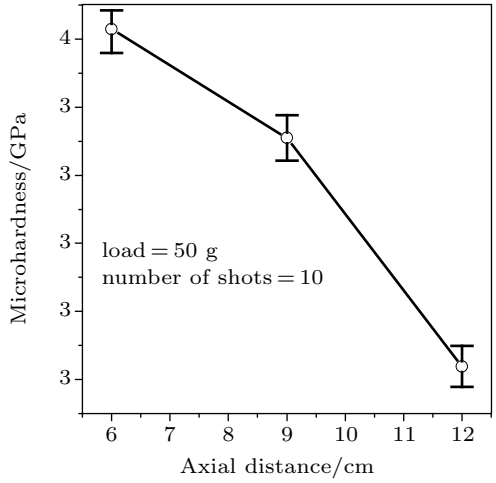


Fig. 13. Values of surface microhardness (GPa) of multiphase ZrO_2 films deposited at different sample axial distances (6 cm, 9 cm, and 12 cm) for 10 focus deposition shots and 1-mbar working gas pressure.

Figure 14 exhibits the values of surface microhardness (GPa) of annealed MZFs. The microhardness of the as-deposited multiphase zirconia film ($\sim 4.2 \pm 0.23$ GPa) increases up to $\sim 5.26 \pm 0.25$ GPa for lower (200 °C) temperature and up to 7.99 ± 0.45 GPa for higher (400 °C) temperature. The increasing trend in microhardness values is due to the phase transformation (from t-ZrO_2 to m-ZrO_2)) and orientation transformation (from m-ZrO_2 (020) to m-ZrO_2 (111)). It is concluded that the major factors that enhance the microhardness of annealed MZFs [add s] are i) rearrangement and re-crystallization of zirconia during its decomposition from t-ZrO_2 phase to m-ZrO_2 phase, ii) overlapping of zirconia (m-ZrO_2) with Zr, iii) increasing oxygen content during continuous annealing, iv) the orientation transformation from m-ZrO_2 (020) to m-ZrO_2 (111), and v) the development of c-ZrO_2 phase.

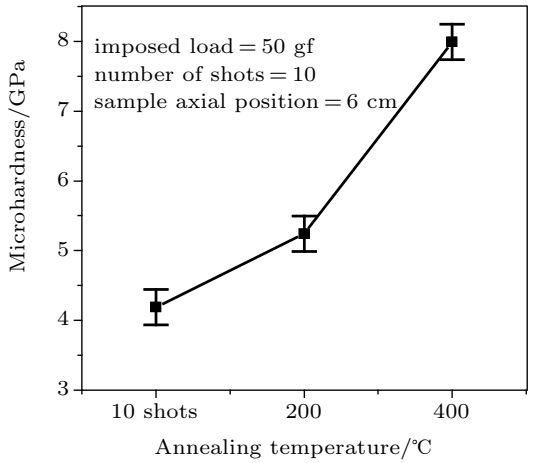


Fig. 14. Values of surface microhardness (GPa) of the as-deposited zirconia films annealed at different temperatures (200 °C and 400 °C).

5. Conclusions

Energetic oxygen ions emanated from PF device are utilized to deposit MZFs. Samples are irradiated for different numbers of focus shots, sample axial distances, and working gas pressures. The focusing efficiency of high voltage signals depends on working gas pressures. Results reveal that 1-mbar pressure is more suitable to deposit MZFs. XRD analysis reveals the formation of polycrystalline MZFs containing (t-ZrO_2, m-ZrO_2, and c-ZrO_2) phases. Maximum crystallinity of t-ZrO_2 phase is observed for 10 focus shots. During continuous (200 °C and 400 °C) annealing, phase transformation occurs (from t-ZrO_2 to m-ZrO_2 and c-ZrO_2). The variations in FWHM, *CS*, and δ are attributed to the relative quantity of incorporated oxygen ions and sample axial distances. At 200-°C AT, FWHM, *CS*, and δ for (020) plane are found to be 0.494, 16.6 nm, and 3.63×10^{-3} nm^{-2} while at 400-°C AT, these parameters for (111) plane are found to be 0.388, 20.87 nm, and 2.29×10^{-3} nm^{-2}, respectively. SEM images demonstrate the formation of rounded grains, showing uniform distribution and the formation of compact MZFs having many patches, which confirms the formation of multi-layered films of multiphase zirconia. For 20-focus shot ion irradiation, comparatively smooth multiphase zirconia film showing rounded grains of uniform distribution is formed. The formations of many patches, cubic, and monoclinic shape of grains and their size are attributed to annealing (200 °C and 400 °C) temperatures. EDX result confirms the presence of Zr (31.12 at.%) and oxygen (65.56 at.%), respectively, in the as-deposited multiphase zirconia film. The estimated values of atomic ratio (O/Zr) in MZFs deposited at 6 cm, 9 cm, and 12 cm are found to be 2.1, 2.2, and 2.3, respectively. FTIR analysis shows that bands appearing at 441 cm^{-1} and 480 cm^{-1} belong to m-ZrO_2 and t-ZrO_2 phases, respectively. Results show that t-ZrO_2 phase is not stable even at low AT while m-ZrO_2 phase is stable even at higher AT but with different orientations. It is concluded that MZFs deposited by PF device are cost effective because no substrate temperature and no trivalent or tetravalent dopants are required to stabilize MZFs.

References

[1] Garvie R C, Hannink R H and Pascoe R T 1975 *Nature* **258** 703
[2] Wilk G D, Wallace R M and Anthony J M 2001 *J. Appl. Phys.* **89** 5243
[3] Wright P K and Evans A G 1999 *Solid State Mater. Sci.* **4** 255
[4] Zhou X, Balachov I and Macdonald D D 1998 *Corros. Sci.* **40** 1349
[5] Nguyen T and Djurado E 2001 *Solid State Ion.* **138** 191
[6] Perkins C M, Triplett B B, Mclntyre P C, Saraswat K C, Haukka S and Tuominen M 2001 *Appl. Phys. Lett.* **78** 2357
[7] Zhao X and Vanderbilt D 2002 *Phys. Rev. B* **65** 075105
[8] Zhao X and Vanderbilt D 2005 *Phys. Rev. B* **71** 085107
[9] Hwang S M, Lee S M, Park K, Lee M S, Joo J, Lim J H, Kim H, Yoon J J and Kim Y D 2011 *Appl. Phys. Lett.* **98** 022903
[10] Panda D and Tseng T-Y 2013 *Thin Solid Films* **531** 1
[11] Piconi C and Maccauro G 1999 *Biomaterials* **20** 1
[12] Namavar F, Wang G, Cheung C L, Sabirianov R, Zeng X C, Mei W N, Bai J, Brewer J R, Haider H and Garvin K L 2007 *Nanotechnology* **18** 415702
[13] Sattonnay G and Thome L 2006 *J. Nucl. Mater.* **348** 223
[14] Chraska T, King A H and Berndt C C 2000 *Mater. Sci. Eng. A* **286** 169
[15] Aguilar D H, Torres-Gonzalez L C, Torres-Martinez L M, Lopez T and Quintana P 2000 *J. Solid State Chem.* **158** 349
[16] Lee S, Tou T Y, Moo S P, Eissa M A, Gholap A V, Kwek K W, Mulyodrono S, Smith A J, Suryadi S, Usada W and Zakaullah M 1988 *Am. J. Phys.* **56** 62
[17] Ahmad R, Sadiq M, Hussain S, Shafiq M, Zakaullah M and Waheed A 2006 *Rev. Sci. Instrum.* **77** 013504
[18] Bhuyan H, Favre M, Valderrama E, Chuaqui H and Wyndham E 2006 *J. Phys. D: Appl. Phys.* **39** 3596
[19] Rawat R S, Srivastava M P, Tandon S and Mansingh A 1993 *Phys. Rev. B* **47** 4858
[20] Rawat R S, Arun P, Videshwar A G, Lam Y L, Lee P, Liu M H, Lee S and Huan A C H 2000 *Mater. Res. Bull.* **35** 477
[21] Rawat R S, Arun P, Videshwar A G, Lee P and Lee S 2004 *J. Appl. Phys.* **95** 7725
[22] Borthakur T K, Sahu A, Mohanty S R, Nayak B B and Acharya B S 1999 *Surf. Eng.* **15** 55
[23] Gupta R and Srivastava M P 2004 *Plasma Sour. Sci. Technol.* **13** 371
[24] Kant C R, Srivastava M P and Rawat R S 1997 *Phys. Lett. A* **226** 212
[25] Rawat R S, Lee P, White T, Ling L and Lee S 2001 *Surf. Coat. Technol.* **138** 159
[26] Hassan M, Qayyum A, Ahmad R, Murtaza G and Zakaullah M 2007 *J. Phys. D: Appl. Phys.* **40** 769
[27] Khan I A, Hassan M, Ahmad R, Qayyum A, Murtaza G, Zakaullah M and Rawat R S 2008 *Thin Solid Films* **516** 8255
[28] Khan I A, Hassan M, Ahmad R, Murtaza G, Zakaullah M, Rawat R S and Lee P 2008 *Int. J. Mod. Phys. B* **22** 3941
[29] Khan I A, Hassan M, Hussain T, Ahmad R, Zakaullah M and Rawat R S 2009 *Appl. Surf. Sci.* **255** 6132
[30] Nayak B B, Acharya B S, Mohanty S R, Borthakur T K and Bhuyan H 2001 *Surf. Coat. Technol.* **145** 8
[31] Ahmad R, Hassan M, Murtaza G, Akhter J I, Qayyum A, Waheed A and Zakaullah M 2006 *Rad. Eff. Deff. Solids* **161** 121
[32] Choi P, Deeney C, Herold H and Wong C S 1990 *Laser Part. Beams* **8** 469
[33] Sadowski M, Schmidt H and Herold H 1981 *Phys. Lett. A* **83** 435
[34] Williamson G B and Smallman R C 1956 *Philos. Mag.* **1** 34
[35] Wang X S, Wu Z C, Webb J F and Liu Z G 2003 *Appl. Phys. A* **77** 561
[36] Khan Z R, Zulfequar M and Khan M S 2010 *Mater. Sci. Eng. B* **174** 145
[37] Khan Z R, Khan Mohd Shoeb, Zulfequar M and Khan Mohd Shahid 2011 *Mater. Sci. Appl.* **2** 340
[38] Kelly H, Lepone A and Marquez A 1998 *IEEE Trans. Plasma Sci.* **26** 113
[39] Nunomura S, Koga K and Shitarani M 2005 *Jpn. J. Appl. Phys. Part II* **44** L1509
[40] Lee S and Saw S H 2012 *Phys. Plasmas* **19** 112703
[41] Sadiq M, Shafiq M, Ahmad W, Ahmad R and Zakaullah M 2006 *Phys. Lett. A* **352** 150
[42] Tian G, Huang J, Wang T, He H and Shao J 2005 *J. Appl. Surf. Sci.* **239** 201